Coordinated Control of Distributed Three- and Single-phase Inverters Connected to Three-Phase Three-Wire Microgrids

Danilo I. Brandao, *Member, IEEE*, Lucas S. Araujo, *Student Member, IEEE*, Augusto M. S. Alonso, *Student Member, IEEE*, Geovane L. dos Reis, Eduardo V. Liberado, *Member, IEEE*, and Fernando P. Marafão, *Member, IEEE*

***Abstract*—This paper explores the coordinated strategy named Power-Based Control to properly coordinate grid-tied single- and three-phase distributed energy resources in three-phase three-wire microgrids. By means of a narrowband, low data rate communication, such strategy accommodates current- and voltage-controlled distributed inverters providing proportional sharing of active, reactive and unbalance (negative-sequence) power terms, also offering dispatchable power flow and high power quality at the microgrid's point of common coupling. Regarding the current unbalance compensation, a particular case considering two distributed single-phase inverters is discussed through mathematical analysis in terms of balanced and unbalanced power terms, and experimental results on which the Power-Based Control is applied to demonstrate that this strategy corroborates with Steinmetz principle. Finally, the complete strategy is evaluated in simulation considering the model of a real urban power distribution grid under typical operational conditions.**

***Index Terms*— Current-controlled mode, Hierarchical control, Microgrid, Power sharing, Three-phase converters, Unbalance compensation, Voltage-controlled mode.**

I. INTRODUCTION

THE government guidelines and interventions have encouraged distributed generators (DGs) based on renewable energy sources in low-voltage (LV) networks. The random integration of a large number of single-phase DGs, interconnected with intrinsically unbalanced loads, can lead to new operational challenges, among which the most important issues are voltage regulation and unbalance caused by uneven and bidirectional power flow circulation between the network phases [1],[2].

Thus, the microgrid (MG) model is adopted to accomplish safe and efficient interoperability of DG. A MG behaves as a single entity capable to: *i*) steer power into the grid; *ii*) efficiently exploit DGs through power sharing methods avoiding the undesirable current circulation; *iii*) operate in both grid-connected and islanded operating modes.

Besides, if properly controlled, a MG may contribute to enhance the power quality (PQ) by reducing distribution loss, improving voltage regulation, compensating voltage/current unbalance and harmonics, and so forth [2]. Besides, a general MG must accommodate any sort of distributed energy resources (DERs) in terms of primary energy source, power electronics topology, and control scheme. Usually, DERs can be single- or three-phase converters, which can operate either in voltage-controlled mode (VCM) or current-controlled mode (CCM). These converters may have inherent self-limitations regarding to their hardware and embedded control for processing reactive power, operating under unbalanced conditions, or tracking the maximum power point (e.g., in case of conventional PV inverters). Thus, voltage regulation, voltage/current unbalance compensation and flexible control methodologies of MG are amongst the most recent issues to be properly dealt with [1],[3].

A. Motivation

Several studies have sought ways to diversify the role of DERs in the electrical system, mainly in terms of improving the PQ. The authors of [4] have proposed a flexible control technique that allows the DERs to inject active power into the grid, as well as to operate concomitantly as an active filter. This objective is achieved through the use of conservative power theory (CPT) and compliance factors. Recently, the DERs are updated with grid-support functions and their performance regarding the local improvement of PQ is analyzed in [5]. In [6], a new configuration of multifunctional DERs capable of directly improve current and voltage quality is presented. That is achieved by changing the DER connection with the grid from

This paragraph of the first footnote will contain the date on which you submitted your paper for review.

The authors are grateful to CAPES, CNPq (grant 420850/2016-3), FAPEMIG (grant APQ-02518-16) and FAPESP (grant 2017/24652-8 and 2016/08645-9).

D. I. Brandao, L. S. Araujo and G. L. dos Reis are with the Graduate Program in Electrical Engineering, Federal University of Minas Gerais (UFMG), Brazil; (e-mail: dibrandao@ufmg.br; savoilucas@gmail.com; geovanereis@ufmg.br).

F. P. Marafão and A. M. dos Santos Alonso, are with the Group of Automation and Integrated Systems, São Paulo State University (UNESP), Sorocaba, Brazil; (e-mail: {fernando.marafao; augusto.alonso}@unesp.br). A. M. dos Santos Alonso is also with the Dept. Electric Power Engineering, Norwegian University of Science and Technology (NTNU), Norway.

E. V. Liberado, is with the Group of Bioenergy and Sustainable Energies (Biojoule), São Paulo State University (UNESP), Campus of Rosana, Brazil; (e-mail: verri.liberado@unesp.br).

parallel to series, and vice-versa, through a two-way switch, causing different modes of operation, according to grid electrical disturbances. Advanced control techniques are proposed for multifunctional DERs to improve PQ of the distribution grids through the injection of harmonic and asymmetric currents in [7],[8]. The techniques aim at improving the dynamic response of DER under the disturbances, besides reducing the complexity and the computational effort of implementation. Indeed, some standards drive the interoperability of ancillary services, as reactive power injection in a MG [9], however, most of those techniques act locally at the point of DER connection, and they should be globally coordinated to enhance PQ indices in a critical bus of the network, such as the microgrid point of common coupling (PCC).

Initially, most of the control strategies of DERs applied in microgrids were based on the well-established concept of droop and reverse droop control, and the MGs were proposed without information and communication technology (ICT) infrastructure, only locally adjusting the droop gains [10],[11]. However, conventional droop controllers suffer from drawbacks such as poor frequency and voltage regulation due to their constant deviation from nominal condition, inaccuracy of power sharing among DERs, low stability margin, power line impedance dependence, and slow dynamic response. These disadvantages are accentuated under weak networks like islanded MG operation [12]-[14]. To overcome these problems, decentralized modified droop with stability and adaptive restriction are proposed in [12]. Then, with the emerging of low-bandwidth communication infrastructure, the MG structures based on central controller, and neighboring-communication (i.e., multi-agent system) have become more attractive [15]-[17], because they achieve more accurate power sharing, lower values of voltage and frequency deviation, and flexible energy management and operation of MG. However, centralized architectures have some inherent drawbacks compared to the decentralized ones. Typical examples are lower reliability and more expensive cost because of ICT.

B. Literature Review

The Power-Based Control (PBC) originally emerged to coordinately control DERs in single-phase MGs, and it has undergone improvements over time in order to enhance its benefits. Table I shows the main PBC evolutions over recent years. This dispatchable MG strategy features coordinate regulation of DERs (i.e., slave units) by a master unit located at the PCC, and inherits as main advantages low implementation complexity, minimum requirements in terms of ICT (i.e., narrowband and low data rate communication), not requiring previous knowledge of the network parameters, and it supports the plug-and-play integration of new DERs. The information exchanged among the master and slave units consists in active and reactive power terms that enables PQ enhancement at PCC with low distribution losses.

TABLE I
EVOLUTION OF PBC STRATEGY FOR MG APPLICATION

PBC Gener.	Features	Ref.
PBC-I	Proposed to single-phase MG. Proportional power sharing of active and reactive power among DERs by two scalar coefficients (α_P, α_Q). If extended for three-phase networks, it does not compensate current unbalance. All DERs are considered CCM.	[18]
PBC-II	Proposed to three-phase four-wire MG. It proportionally shares active and reactive power among DERs that are connected at the same *m*-phase and provides current unbalance compensation at the PCC by six scalar phase coefficients α_{Pm} and α_{Qm}, where *m* represents phases *a*, *b* and *c*. The three-phase DERs operate unbalanced. All DERs are considered CCM.	[1]
PBC-III	Proposed to three-phase four-wire MG. It proportionally shares active and reactive power among DERs that are connected at the same *m*-phase and provides current unbalance compensation at the PCC by eight scalar phase coefficients α_{Pm}, α_{Qm}, $\alpha_{P3\Phi}$ and $\alpha_{Q3\Phi}$. The three-phase DERs may operate balanced. All DERs are considered CCM.	[19]

A coordinated control method for CCM and VCM units using a central controller and virtual admittance is proposed in [15]. However, the limited capacity and reactive power sharing of the CCM and VCM units are not considered, as well as the grid power flow control.

The authors of [16] propose a technique to improve the voltage quality in LV distribution power system using the reactive power capacity of single-phase PV inverters. The proposal is tested in three-phase four-wire network with high penetration of PV-based DERs. The method consists in controlling the reactive power injection considering two groups of inverter connections: *1*) the line-to-line connected DERs form an equivalent delta connection device, while *2*) the line-to-neutral connected DERs comprise an equivalent wye connection device. The former group is used to mitigate reactive power, while the latter improves voltage quality. Although, it needs to identify the DERs connection between phases and between phases to neutral, which shows a certain similarity with PBC [1]. It does not consider a heterogeneous MG with single- and three-phase DERs, and nor analysis during islanded operation is performed.

The authors of [17] propose a hierarchical control for power sharing and compensation of voltage unbalance and harmonic current in isolated three-phase AC system, aiming at enhancing the voltage quality of a critical load bus (CLB). The hierarchical control is split into two layers (primary and secondary). The primary layer goals: *1*) to set voltage and frequency to the MG in a decentralized way, and to guarantee proper power balance between generation and load consumption; *2*) to compensate for voltage unbalance and harmonic currents; *3*) to minimize the fundamental and harmonic current terms circulating between the DERs, and *4*) to compensate for mismatch in the voltage drops across the feeders. The DER control method consists of droop control, unbalanced compensation and virtual impedance loop. The use of positive and negative sequence virtual impedances plus harmonic virtual impedance improves the system performance. The secondary control must restore the

frequency and amplitude of the CLB voltage on the basis of a MG central controller that periodically exchanges data through a narrowband communication links. Again, this method resembles the PBC in hierarchical control technique and the CLB corresponds to the MG´s PCC AC bus.

In [20] a distributed and autonomous control of DERs is proposed in both VCM and CCM modes for reactive and harmonic power compensation in an isolated MG perspective. The coordinated control of distributed units is implemented using only local measurements. The results show that harmonic compensation is obtained through virtual admittance and impedance schemes while the reactive power sharing uses the surplus power capacity of DERs. However, it does not consider unbalanced compensation and there is still line impedance influence due to adopted droop control.

Some of the aforementioned approaches, along with other relevant works found in literature, are further explored in Table II, focusing on the matter of unbalance compensation in MGs based on uneven dispersed DERs. Such literature review aims at highlighting the main features of each proposal in terms of: *i*) the main issues tackled; *ii*) how the cooperative control of DERs is implemented; *iii*) the PQ enhancement; *iv*) the adopted MG network and topology of existing DERs; and *v*) the means of assessment of results. Secondly, this result reinforces the contributions of the proposed method, which strives current unbalance compensation using single- and three-phase DERs in both CCM and VCM in three-phase three-wire networks.

TABLE II
COMPARATIVE SUMMARIZATION OF LITERATURE REVIEW ON MG CONTROL

Ref.	***features***			***methodology***					***microgrid***	***result***
	Main goals	**DER topols.**	**MG and communicat. architecture**	**Control approach**	**Power sharing**	**Grid power control**	**PQ compens.**	**DER control mode**	**Topology and # of DERs**	**Exp.**
[1]	Coordination of arbitrary connected single-phase DERs	only 1Φ	centralized control with narrowband communication	model-free PBC-II	Good	Yes	Reactive and load unbalance	only CCM	Radial(3P4W) 14 Nodes 6 DERs	No
[15]	Reduction of voltage harmonic distortion at PCC	only 3Φ	centralized control with communication	virtual admittance	Fair	No	Harmonic voltage	both CCM and VCM	Radial (3P3W) islanded 6 Nodes 2 DERs	Yes
[16]	Voltage unbalance compensation and regulation	only 1Φ	decentralized with sparse and narrowband communication	consensus-based algorithm	Good	No	Reactive / voltage unbalance / voltage regulation	only CCM	Radial(3P4W) 55 Nodes 55 DERs	No
[17]	Voltage unbalance harmonic compensation	only 3Φ	hierarchical control with low bandwidth communication	droop control, virtual impedance	Good	No	Reactive / harmonic	only VCM	Radial(3P3W) islanded 4 Nodes 2 DERs	No
[20]	Voltage harmonic compensation	only 3Φ	decentralized/ without communication	direct and reverse droop control with virtual admittance	Fair	No	Reactive / harmonic voltage	both CCM and VCM	Radial(3P3W) islanded 4 Nodes 3 DERs	Yes
[21]	Voltage unbalance compensation	only 3Φ	decentralized/ without communication	droop control, virtual impedance	Fair	No	Reactive & unbalance voltage	only VCM	Radial(3P3W) islanded 3 Nodes 2 DERs	Yes
[22]	Voltage unbalance compensation	only 3Φ	decentralized/ without communication	droop control,	Poor	No	Reactive & unbalance voltage	only VCM	Radial(3P3W) 3 Nodes 2 DERs	Yes
[23]	Voltage Unbalance Compensation	only 3Φ	hierarchical control with narrowband communication	droop control, virtual impedance	Fair	No	Reactive & unbalance voltage	only VCM	Radial(3P3W) islanded 3 Nodes 2 DERs	No
[24]	Enhancement of voltage quality at the MG´s PCC	only 3Φ	hierarchical control with narrowband communication	Droop control, virtual impedance	Poor	No	Reactive & unbalance voltage	only VCM	Radial(3P3W) islanded 3 Nodes 2 DERs	No
[25]	Harmonic compensation and voltage support	only 3Φ	decentralized/ with narrowband communication	multi-loop control, virtual admittance	Good	No	Reactive / harmonic voltage	only CCM	Radial(3P3W) 6Nodes 2 DERs	Yes
Here	Current unbalance compensation and accurate power sharing.	both 3Φ and 1Φ	centralized control with narrowband communication	model-free PBC	Good	Yes	Reactive and load unbalance	both CCM and VCM	Radial(3P3W) 14 Nodes 6 DERs	Yes

*3P3W and 3P4W means three-phase three- and four wire system; poor, fair and good power sharing means, respectively, inaccurate, accurate with demand on network parameters and accurate with no requirement of previous knowledge of the network parameters.

C. Contribution and Paper Organization

Considering the recent methods of centralized control strategies described previously, this paper proposes a coordinated control applied to three-phase three-wire MGs that allows: *i*) tight grid power flow control; *ii*) proportional power sharing; and *iii*) unbalance compensation in both grid-connected and islanded modes. Consequently, accurate sharing of active and reactive power among single- and three-phase DERs operating in both VCM and CCM is achieved.

The innovative contribution of this paper is proposing an improved PBC algorithm capable of controlling three-phase DERs coexisting with single-phase ones and considering their topology/control features, thus approaching a real case application in three-phase three-wire network. This strategy enables to arrange a flexible MG control method on which the DERs may operate in different ways: #1) three-phase DERs that must operate balanced, proportionally contributing to active and reactive power sharing; #2) single or three-phase DERs operating in both VCM and CCM; #3) explore the fact that with only two single-phase DERs, connected in different phases, it is possible to compensate three-phase three-wire load unbalance, in accordance with Steinmetz principle [21]. To the best of the authors' knowledge, no hierarchical control strategy capable of all those above-mentioned features was presented in the literature previously. Finally, this paper is the continuation of [1] coping with the stated future works.

This paper is organized as follow. Section II presents the MG elements and its local control scheme and structures. Section III goes through the three levels of the hierarchical control, and PBC devised in the secondary-level, as well its stability analyses. Section IV provides the analytical decomposition of balanced and unbalanced power terms to the power unbalance compensation. Section V shows simulation results considering a more complete scenario similar to a real urban distribution power system and with the MG operating in isolated mode, while Section VI validates the method through a laboratory-scale prototype. Finally, Section VII presents the main conclusions.

II. Microgrid Elements and Structure

The considered MG structure is shown in Fig. 1. It represents a part of a real three-phase three-wire metropolitan distribution power system with aerial cables. The three-phase three-wire LV networks can be found in some parts of Africa, Central America, Asia and Europe, e.g., Norway [27],[28].

Two classes of active components comprise the existing *master/slave* architecture: a centralized utility-interactive converter (i.e., endowed with the master controller – MC) and DERs (i.e., slave units). The former operates as a grid-supporting converter during MG grid-connected mode, whereas it operates as grid-forming converter when the MG is islanded. Such converter, named *Utility Interface* (UI), also guarantees smooth transition between MG modes of operation [29]. The latter components can be further classified as grid-connected inverters operating in CCM and VCM. Such devices consist of DERs equipped with any sort of primary energy source (PES) (e.g., solar or wind) associated with battery, and a communication module. A narrowband, low data rate communication link interconnects the slave units to the MC. Finally, the linear and nonlinear loads are the MG's passive components. The control scheme of the single- (1Φ) and three-phase (3Φ) DERs, under both CCM and VCM, are devised in *abc*-frame as shown in Fig. 2, described as follows:

1) *The 1Φ current-based DERs* are usually applied to residential installation with small power generation, i.e., lower than 10-15 kW [30]. Due to its single-phase connection and the intermittent generation of renewables, such converter topology may increase the unbalance in three-phase distribution networks. Contrariwise, if properly controlled and there being available power capacity, they can cooperatively contribute to unbalance compensation without loss of performance. The control scheme of a current-based DER comprises of an inner inductor-current control and an outer power control loop. Then the inverter tracks a precise instantaneous current reference, which is given by the power loop, so as it can be modeled as a controlled-current source.
2) *The 1Φ voltage-based DERs* comprise the triple loop control with an inner inductor-current control, an output capacitor voltage control, and an outer power control loop. If properly designed [31], the inverter tracks a precise instantaneous voltage reference within a certain frequency band. The utility-interactive inverter is a sort of voltage-based converter properly designed to operate as a centralized converter according to [29].
3) *The 3Φ current-based DERs* are usually applied to industrial installation with power generation larger than 15 kW. It is

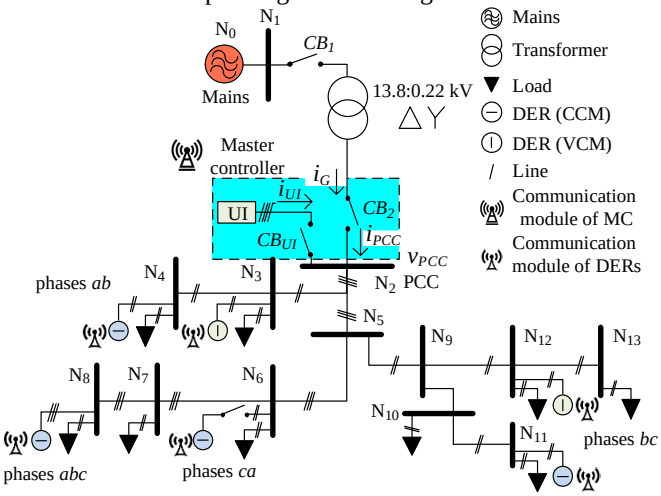

Fig. 1. Three-phase three-wire microgrid structure with single- and three-phase distributed units, considering CCM DERs, VCM DERs and loads.

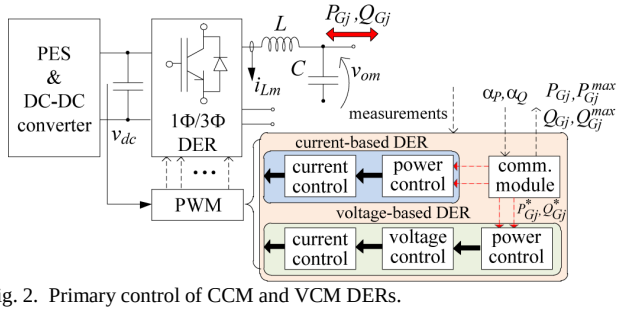

Fig. 2. Primary control of CCM and VCM DERs.

crucial that three-phase DERs operate balanced in order to avoid instantaneous power fluctuation because they are typically designed with small DC capacitors. Then, the control scheme of such *3Φ* DER is like a *1Φ* one, just adapting the outer power loop to manage three-phase active/reactive power. Since the control of inverters is sufficiently studied in the literature it is not focused herein.

In Fig. 1, each of the circular elements (i.e., DERs) represents the structure highlighted in Fig. 2 (CCM or VCM). The power variables are calculated based on the local variables measured on the point of DER connection with the grid. Note that all DERs are single-phase except for DER connected at node N_8.

III. Hierarchical Control and Power-Based Control

The adopted hierarchical MG control approach is basically split into three layers as shown in Fig. 3. This division is done according to the update frequency rate of the handled variables, also upon the imperativeness of the layer for the system overall adequate operation.

The primary layer is the fastest one, working on the kHz scale, and it is responsible for the local operation of DERs and UI. This layer includes the basic and specific functions, which are the elementary operational functions of the converter to work according to standardized requirements, such as the current and voltage control, DC link control, and grid synchronization. The smooth transition between connected and isolated modes is implement at the UI. Depending on the PES and local grid codes, there are some specific functions for each of them [32]. Ancillary services are complementally offered, being not vital for the converter operation. It is worth underlining that local controllers guarantee compliance with grid codes, and do not rely on the communication link.

The secondary layer comprises the PBC algorithm and it is executed based on a fundamental frequency rate (≈20 ms). This layer works toward the proportional power sharing, where the power quantities of each DER are sent to the MC, which thereupon broadcasts the new portion of power that each DER shall provide, according to their capability. Hence, the secondary layer is dependent on communication; however, if the communication is lost, the MG still operates assuming the functionalities of the primary layer.

The tertiary layer is the slowest, being updated few times per day. It is responsible for defining the references for the active or reactive power flow between the MG and the main grid, therefore it only works under interconnected mode. This layer allows the interaction with the utility's distribution system operator (DSO), in terms of active and reactive power flow. Note that there is no control loop in this layer; it just generates the active and reactive power references based on technical or economic interests within the mutual agreed contract.

A. General Power-Based Control

The PBC does not require previous knowledge of network parameters. Besides of its simplicity, it achieves a robust control of DERs to allow: *i*) power flow control at the grid side of PCC; *ii*) accurate proportional power sharing; *iii*) high level of PQ, and iv) compliance with grid codes. The innovative aspect of the PBC described in this work is its application in a scenario on which balanced three-phase DERs coexist with single-phase DERs operating as CCM or VCM. Thus, three-phase DERs contribute proportionally to active feed-in and reactive mitigation, avoiding DC voltage fluctuation at their DC-link; while single-phase DERs contribute to active feeding and to reactive and unbalance (negative-sequence) compensation. The harmonics are reduced by the UI converter itself [29].

For the sake of understanding, the PBC is split into: 1) data packet sent from DERs to MC; 2) PBC algorithm processed on the MC and scaling coefficients broadcasted to DERs; 3) DER's local power reference calculation. Fig. 4 schematically summarizes the cyclic operational steps of the PBC algorithm.

1) Data Packet from DERs to Master Controller

The control is performed considering the time-varying status of distributed units, which is collected by the MC at the beginning of each control cycle period (l). The status of a j-th DER (j = 1, 2, …, J) is a set of power quantities representing the related capacity to process and generate power, including: its actual active [$P_{Gj}(l)$] and reactive [$Q_{Gj}(l)$] output power; its

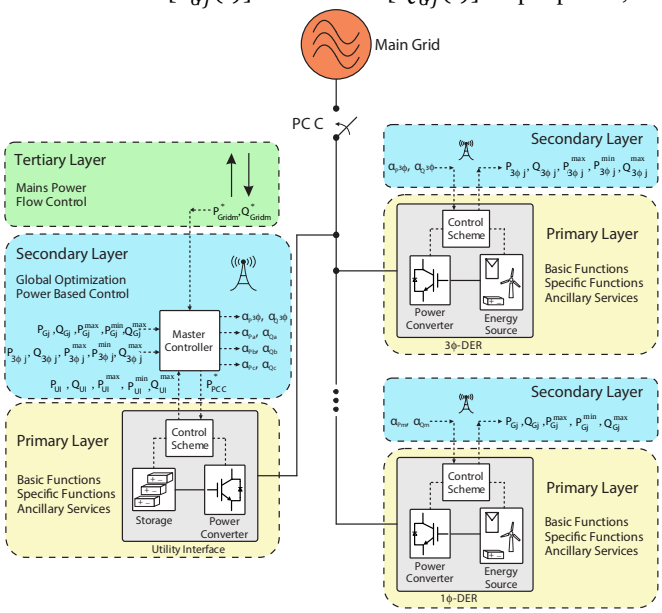

Fig. 3. Microgrid hierarchical control scheme based on Power-Based Control.

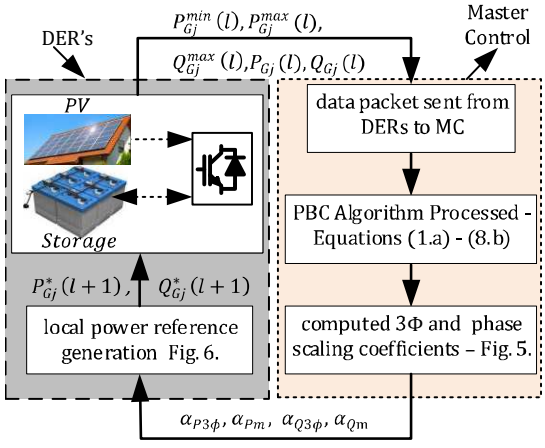

Fig. 4. Flowchart with the proposed PBC execution sequence.

maximum capacity to provide active $[P_{Gj}^{max}(l)]$ and reactive $[Q_{Gj}^{max}(l)]$ power, given by (1), where $A_{Gj}(l)$ is the rated apparent power of DERj; and, if local storage is presented, the maximum active power the DER can absorb from the grid $[P_{Gj}^{min}(l)]$, given by a negative value.

$$Q_{Gj}^{max}(l) = \sqrt{A_{Gj}(l)^2 - P_{Gj}(l)^2} \quad (1)$$

2) PBC Algorithm Processed into the Master Controller

Once the MC has gathered all the required information, the status of the whole MG is computed in terms of the power quantities introduced in the following steps. Let us indicate with *m* a generic phase of a three-phase system, and with *3Φ* any three-phase quantities for three-phase balanced devices. Then, the mentioned steps and computed quantities are:

Step 1 – total active and reactive power delivered by the three- $[P_{G3\phi t}(l), Q_{G3\phi t}(l)]$ and single-phase $[P_{Gmt}(l), Q_{Gmt}(l)]$ DERs along cycle *l*:

$$P_{G3\phi t}(l) = \sum_{j=1}^{J} P_{G3\phi j}(l) \quad (2.a)$$

$$Q_{G3\phi t}(l) = \sum_{j=1}^{J} Q_{G3\phi j}(l) \quad (2.b)$$

$$P_{Gmt}(l) = \sum_{j=1}^{J} P_{Gmj}(l) \quad (2.c)$$

$$Q_{Gmt}(l) = \sum_{j=1}^{J} Q_{Gmj}(l) \quad (2.d)$$

Similarly, the total minimum $[P_{G3\phi t}^{min}(l),\ P_{Gmt}^{min}(l)]$ and maximum $[P_{G3\phi t}^{max}(l),\ P_{Gmt}^{max}(l)]$ active power, and the total maximum $[Q_{G3\phi t}^{max}(l),\ Q_{Gmt}^{max}(l)]$ reactive power of three- and single-phase DERs are calculated.

Step 2 – the total capacity of active and reactive power available for contributing to the whole MG power needs:

$$P_{Gt}^{max}(l) = P_{G3\phi t}^{max}(l) + \sum_{m=1}^{M} P_{Gmt}^{max}(l) \quad (3.a)$$

$$Q_{Gt}^{max}(l) = Q_{G3\phi t}^{max}(l) + \sum_{m=1}^{M} Q_{Gmt}^{max}(l) \quad (3.b)$$

Step 3 – the total active $[P_{Lmt}(l)]$ and reactive $[Q_{Lmt}(l)]$ power demanded by the MG per phase within the cycle *l*, disregarding the three-phase DERs:

$$P_{Lmt}(l) = P_{gridm}(l) + P_{UIm}(l) + P_{Gmt}(l) \quad (4.a)$$

$$Q_{Lmt}(l) = Q_{gridm}(l) + Q_{UIm}(l) + Q_{Gmt}(l) \quad (4.b)$$

where P_{gridm} and Q_{gridm} are the phase active and reactive power measured at the grid side of the PCC, and P_{UIm} and Q_{UIm} are the phase active and reactive power delivered by the UI;

Step 4 – the total three-phase active $[P_{Lt}(l)]$ and reactive $[Q_{Lt}(l)]$ power processed within the MG during cycle *l*:

$$P_{Lt}(l) = \sum_{m=1}^{M} [P_{Lmt}(l)] + P_{G3\phi t}(l) \quad (5.a)$$

$$Q_{Lt}(l) = \sum_{m=1}^{M} [Q_{Lmt}(l)] + Q_{G3\phi t}(l) \quad (5.b)$$

note that the distribution power loss through line impedances is considered in $P_{Lmt}(l)$ and $P_{Lt}(l)$, likewise any other distributed inverter not participating in the PBC.

Step 5 – possessing the total power absorbed and generated in the MG, the MC calculates the references for the total three-phase active $[P_{G3\phi t}^{*}(l+1)]$ and reactive $[Q_{G3\phi t}^{*}(l+1)]$ power to be delivered by the three-phase balanced DERs in the next control cycle *l*+1, and the references for the total phase active $[P_{Gmt}^{*}(l+1)]$ and reactive $[Q_{Gmt}^{*}(l+1)]$ power to be provided by the single-phase DERs:

$$P_{G3\phi t}^{*}(l+1) = P_{Lt}(l) - \sum_{m=1}^{M} P_{PCCm}^{*}(l+1) \quad (6.a)$$

$$Q_{G3\phi t}^{*}(l+1) = Q_{Lt}(l) - \sum_{m=1}^{M} Q_{PCCm}^{*}(l+1) \quad (6.b)$$

$$P_{Gmt}^{*}(l+1) = P_{Lmt}(l) - P_{PCCm}^{*}(l+1) \quad (6.c)$$

$$Q_{Gmt}^{*}(l+1) = Q_{Lmt}(l) - Q_{PCCm}^{*}(l+1) \quad (6.d)$$

where $P^{*}_{PCCm}(l+1)$ and $Q^{*}_{PCCm}(l+1)$ are, respectively, the active and reactive references of the phase power flow at the PCC determined by the tertiary control layer. Upon setting such references, $P_{G3\phi t}^{*}$, $Q_{G3\phi t}^{*}$, P_{Gmt}^{*}, and Q_{Gmt}^{*} come as consequence. These DER related references are selected by the MC to regulate the power flow at the MG's PCC among the different phases, according to the energy state of the UI and DERs. Note that they are estimated, for a next control cycle, based on the quantities measured during the actual cycle (*l*).

Step 6 – considering the polarities of Fig. 1, the exchanged power at the terminals of the UI are:

$$P_{UIm}(l+1) = P_{PCCm}^{*}(l+1) - P_{gridm}^{*}(l+1)\,, \quad (7.a)$$

$$Q_{UIm}(l+1) = Q_{PCCm}^{*}(l+1) - Q_{gridm}^{*}(l+1)\,. \quad (7.b)$$

where the grid power references P_{gridm}^{*} and Q_{gridm}^{*} guarantee the balanced condition at the grid side, being set based on long term energy management strategies (e.g., negotiations with the DSO) or set to zero in islanded mode.

Step 7 – Finally, the *3Φ* scaling coefficients $\alpha_{P3\phi}$ and $\alpha_{Q3\phi}$, and the *m*-phase scaling coefficients α_{Pm} and α_{Qm} (all ranging in the interval [-1, 1]) are computed and broadcasted to all the DERs. $\alpha_{P3\phi}$ and $\alpha_{Q3\phi}$ are sent to three-phase balanced devices only, while α_{Pm} and α_{Qm} are broadcasted to single-phase units

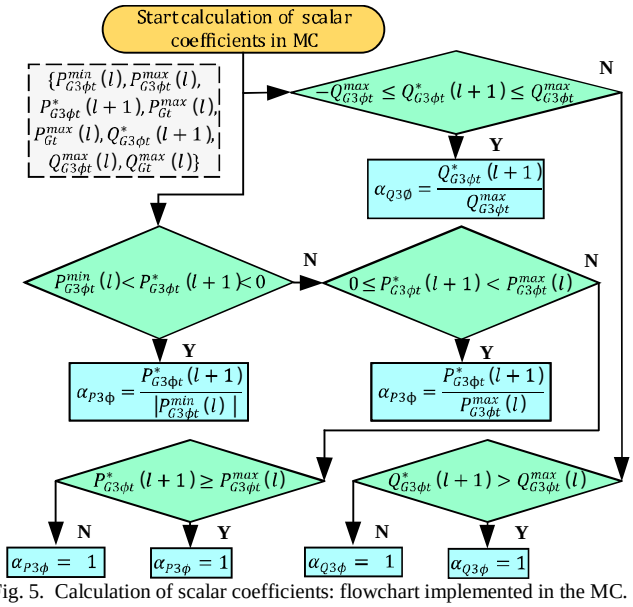

Fig. 5. Calculation of scalar coefficients: flowchart implemented in the MC.

connected to the corresponding *m*-phase. The active power is controlled by variable α_P, while the reactive power is controlled by variable α_Q. Fig. 5 shows the flowchart with the calculation procedure for coefficients.

3) Power Reference Generator of DER local controller

Thus, given α_P and α_Q, the *j-th* DER controls its local active and reactive power injection according to Fig. 6. It is worth underlining that coefficients are properly saturated, which prevents overcurrent stresses in steady-state, and active power injection takes precedence over the reactive power exchange as noted in (1).

In Fig. 6, $P^*_{Gj}(l+1)$ and $Q^*_{Gj}(l+1)$ are respectively the active and reactive power references for DER_j in the next control cycle. The negative and positive signals of α_P and α_Q represents, respectively, storage and delivery of active power, and capacitive and inductive reactive power. Besides, Fig. 6, holds for both grid-connected and islanded operation. Regarding the islanded mode, if the uncontrolled DERs generate more active power than the MG can absorb (including energy storage systems), then, their local controllers shall be able to adjust the power to be injected into the grid accordingly to the requirement for primary services of frequency and voltage regulation [33].

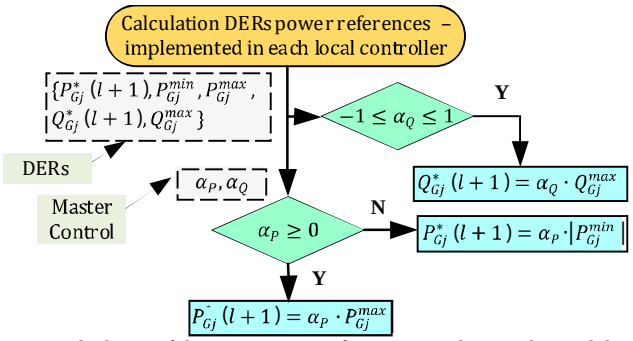

Fig. 6. Calculation of the DERs power references - implemented in each local controller of DER.

B. Stability Analysis

This section presents the stability analysis of the proposed coordinated strategy based on the PBC implementation. A simplified block diagram representing the main operations of the PBC for what concerns active power balance is shown in Fig. 7; a corresponding scheme can be derived for reactive power control. Time-delay in communications between MC and DERs, and vice-versa, namely T_d, is inherent to the PBC methodology and it is included to take into account the phase margin deviations and to assess system stability.

The scheme in Fig. 7(a) highlights the MC, communication infrastructure, DER local controller, and MG power system parts. The PBC in the MC is continuously processed within a time processing of period *T*. Yet, Fig. 7(b) is employed to derive the discrete time transfer function between the total absorbed power, P_{Lm}, and the reference, P^*_{Gmt} (8). The variables T_d and ω_c correspond to the communication time-delay and bandwidth of the local controller of DERs (i.e., $\omega_c = 2.\pi.15$, considering an external power loop for both CCM and VCM, as shown in Fig. 2), respectively. The reference input P^*_{PCCm} is neglected, since it varies very slowly as mentioned in Section III. Thus, the system stability is evaluated considering two main issues: 1) variation of time-delay, T_d, and 2) variation of PBC time-processing, *T*. The results are shown in Fig. 8.

$$P^*_{Gmt}(z) = \frac{P_{Lm}(z)}{z + H_{\omega_c}(z).T_d(z)[1 - T_d(z)]} \quad (8)$$

By mapping the poles ("×") and zeros ("○") of the system, it can be noticed that T_d and *T* affect the behavior of the model distinctively in regard to stability. Firstly, in Fig. 8(a) the system is assessed considering T_d varying from 1/600 s up to 1/6 s, while considering *T* = 1/60 s. Note that the system can be considered stable for all the considered values of T_d, since all poles lie within the unit circle. Hence, by considering that modern communication systems applied to such scenario could present maximum latency of about 100 ms [34], the PBC operation would not impair in instability. The drawback of having slower transmission times for the data flowing from DERs to MC (i.e., higher T_d); however, is that the poles of the system tend to move towards the positive real axis, becoming more dominant and consequently presenting more influence on system stability. In addition, as T_d becomes higher, the zeros of the system tend to move to the boundary of the unit circle and might extrapolate it as well. Although such zeros outside the stability region do not affect the overall performance of the system, they potentially introduce non-minimum phase features, which may limit control bandwidth and decrease the phase margin [35].

The influence of increasing *T* is presented in Fig. 8(b). It is now considered T_d = 1/120 s and *T* varying from 1/600 s to 1/6 s. Different from the previous case, slower transmission times from the MC to DERs introduce a tendency of having dominant poles lying on the negative real axis. With all poles within the unit circle, such condition also does not affect stability, although by being on the left half-plane there is an indication of more oscillatory behavior of the system [35]. This result is reasonable since the time response of the system is

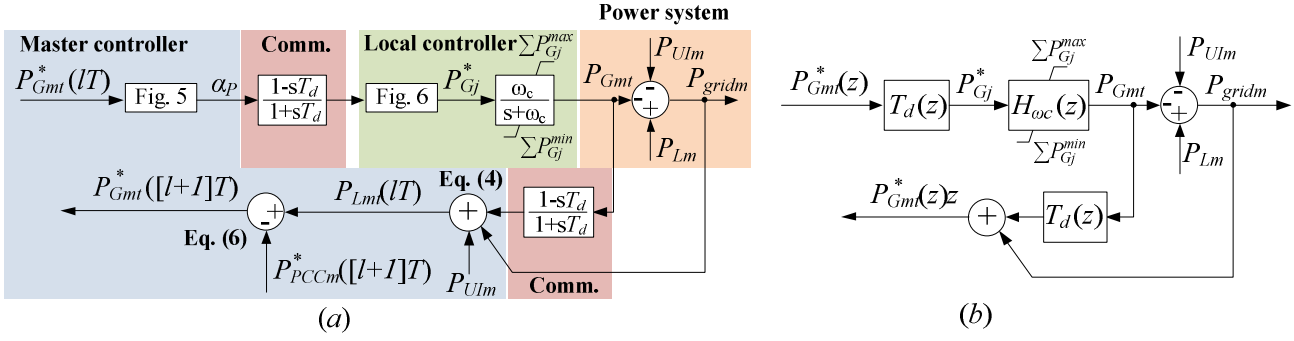

Fig. 7. Simplified model of the Coordinated Control approach based on the PBC for distributed three- and single-phase inverters.

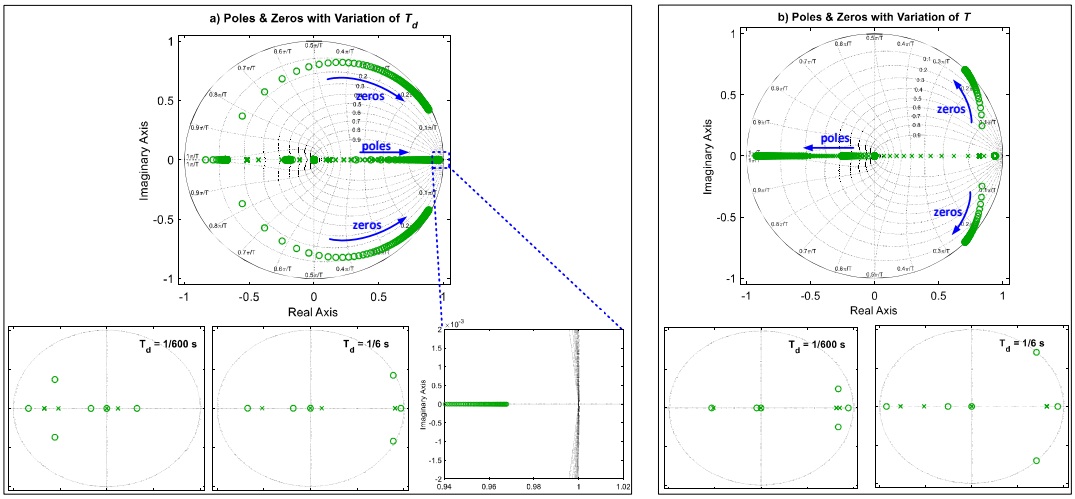

Fig. 8. System behavior and pole and zero mapping considering different communication delays and slower MC time processing: variation of (a) Td and (b) T.

directly dependent on the processing/transmission time of the control coefficients calculated by the PBC and which must be broadcasted to DERs to respond adequately. Again, zeros tend to exceed the unit circle boundary as the *T* increases.

IV. Analytical Decomposition of Balanced and Unbalanced Components of Power

This section presents a mathematical modeling for unbalanced operation of three-phase networks. Considering a three-phase three-wire MG for which the fundamental frequency phase voltages and their rms values are expressed by the vectors:

$$\underline{v} = [v_a \quad v_b \quad v_c]^T, \qquad \underline{V} = [V_a \quad V_b \quad V_c]^T \tag{9}$$

The phase voltages can be obtained from the measured line-to-line voltages by using:

$$v_{m=a,b,c} = \frac{1}{3}\sum_{n=a,b,c} v_{mn}, m \neq n \tag{10}$$

Similarly to (9), let $\underline{P}$ and $\underline{Q}$ be the vectors of phase active and reactive power absorbed by the MG, such that $P_{3\phi} = \underline{1}^T\underline{P}$ and $Q_{3\phi} = \underline{1}^T\underline{Q}$ are the total active and reactive power at the MG, $\underline{1}$ is the unity vector and ^{T} means transpose.

Based on the above definitions, the active and reactive power can be decomposed into balanced and unbalanced components through the following expressions:

$$\underline{P}^b = \frac{P_{3\phi}}{V_a^2+V_b^2+V_c^2}\begin{bmatrix}V_a^2\\V_b^2\\V_c^2\end{bmatrix} \tag{11.a}$$

$$\underline{Q}^b = \frac{Q_{3\phi}}{V_a^2+V_b^2+V_c^2}\begin{bmatrix}V_a^2\\V_b^2\\V_c^2\end{bmatrix} \tag{11.b}$$

$$\underline{P}^u = \underline{P} - \underline{P}^b \tag{11.c}$$

$$\underline{Q}^u = \underline{Q} - \underline{Q}^b \tag{11.d}$$

The balanced components correspond to the active (or reactive) power absorbed by each phase of a balanced load with the same total active (or reactive) power flow of the MG, i.e.,

$$\sum_{m=a,b,c} P_m^b = P_{3\phi} \tag{12.a}$$

$$\sum_{m=a,b,c} Q_m^b = Q_{3\phi} \tag{12.b}$$

On the other hand, the unbalanced power components are related to the difference between the actual power absorption in each phase of the MG and the corresponding power that would be absorbed by an equivalent balanced load, irrespective of voltages. Moreover, in three-phase three-wire systems:

$$\sum_{m=a,b,c} P_m^u = 0 \quad , \quad \sum_{m=a,b,c} Q_m^u = 0 \tag{13}$$

From (13), observe that for full compensation of unbalanced components, these quantities could be calculated for just two (out of the three) phases of the MG and, in the context of this work, addressed to single-phase compensators.

Consider now the Steinmetz compensation approach, defined for three-phase three-wire circuits supplied by fundamental-frequency positive-sequence voltages [26]. In this scenario, the power components to be addressed to line-to-line power converters are expressed by the vector:

$$\underline{Q}^* = [Q_{ab}^* \quad Q_{bc}^* \quad Q_{ca}^*]^t \tag{14}$$

Thus, full compensation of unbalanced active and reactive power components can be achieved by defining $\underline{Q}^*$ such that it minimizes both $\underline{P}^u$ and $\underline{Q}^u$. By solving the resulting minimization problem, the following expression is obtained:

$$\begin{bmatrix}Q_{ab}^*\\Q_{bc}^*\\Q_{ca}^*\end{bmatrix} = \left(\frac{1}{\sqrt{3}}\begin{bmatrix}1&-1&0\\0&1&-1\\-1&0&1\end{bmatrix}\cdot\underline{P}^u + \frac{1}{3}\begin{bmatrix}2&2&-1\\-1&2&2\\2&-1&2\end{bmatrix}\cdot\underline{Q}^u\right) \tag{15}$$

Observe that, if the load is purely resistive and unbalanced (as described in [26]), a complete unbalanced compensation is achieved by calculating two elements of $\underline{Q}^*$ from (15) and addressing them to two line-to-line compensators.

If a set of three line-to-line DERs is available, their active power reference signals can be calculated in terms of $\underline{P}$ or $\underline{P}^b$, indicated as follows:

$$\underline{P}^* = \begin{bmatrix}P_{ab}^*\\P_{bc}^*\\P_{ca}^*\end{bmatrix} = \begin{bmatrix}1&1&-1\\-1&1&1\\1&-1&1\end{bmatrix}\cdot\underline{P} \tag{16.a}$$

$$\underline{P}^* = \begin{bmatrix}P_{ab}^*\\P_{bc}^*\\P_{ca}^*\end{bmatrix} = \begin{bmatrix}1&1&-1\\-1&1&1\\1&-1&1\end{bmatrix}\cdot\underline{P}^b \tag{16.b}$$

The difference between (16.a) and (16.b) is that the unbalanced active power components caused by load unbalance are considered only in (16.a). Correspondingly, if the three line-

to-line DERs can provide reactive power to the load, $\underline{Q}^*$ can be calculated considering both unbalanced and balanced reactive power (17.a) or just the balanced reactive power (17.b):

$$\underline{Q}^* = \begin{bmatrix} Q^*_{ab} \\ Q^*_{bc} \\ Q^*_{ca} \end{bmatrix} = \begin{bmatrix} 1 & 1 & -1 \\ -1 & 1 & 1 \\ 1 & -1 & 1 \end{bmatrix} \cdot \underline{Q} \qquad (17.a)$$

$$\underline{Q}^* = \begin{bmatrix} Q^*_{ab} \\ Q^*_{bc} \\ Q^*_{ca} \end{bmatrix} = \begin{bmatrix} 1 & 1 & -1 \\ -1 & 1 & 1 \\ 1 & -1 & 1 \end{bmatrix} \cdot \underline{Q}^b \qquad (17.b)$$

Alternatively, (15) could be used instead of (17.a) or (17.b) by replacing the term $\underline{Q}^u$ in (15) by $\underline{Q}$. In this case, only (16.b) should be considered for active power control, since that the unbalanced active power is already included in (15).

Also, since that the supply voltages have only positive-sequence component (from which results that $V_a = V_b = V_c$), one may note from (11.a) and (11.b) that the balanced power components would have the same value, i.e., $P_a^b = P_b^b = P_c^b = P_{PCC3\phi}/3$. Therefore, (17.a) can be rewritten as:

$$\underline{P}^* = \frac{P_{PCC3\phi}}{3} \cdot \underline{1} \qquad (18)$$

In conclusion, for non-ideal voltages (i.e., asymmetry and harmonic distortion), (15)-(17) can be rewritten as a function of the internal product of the supply voltages. In addition, the proposed decomposition remains valid for the active power (indeed, the balanced active power may have different values in the three phases), but not for the reactive power, which must be replaced by the reactive energy, which is a conservative quantity defined in [36].

V. Simulation Results

A. MG in islanded mode operation

The simulation results assess the proposed PBC strategy in a general scenario, considering an urban distribution power system, as shown in Fig. 1, with the MG operating in islanded mode, i.e., CB_2 is opened ($P^*_{gridm} = Q^*_{gridm} = 0$). Thus, different case studies are carried out in order to: *i*) show how the proposed method accommodates CCM and VCM DERs; *ii*) demonstrate the PBC regulating single- and three-phase inverters; and *iii*) verify that at least two DERs connected at different phases are enough to compensate the active and reactive power unbalance by their own, when they have available capability. The set of full-bridge inverter legs, output *L* filter, PWM and inner current control loop of DERs is modeled as an ideal current source with a small shunt capacitor. The outer power and voltage/power control loops described in Section II for both CCM and VCM DERs are devised as well.

The MG is connected at node N_2, which represents the MG´s PCC, and presents a nominal power of 60 kVA considering linear and nonlinear loads. The non-homogeneous line impedance values used in the network are shown in Table III, while the parameters of DERs are shown in Table IV. When the MG operates in islanded mode, the voltage and frequency references are provided by the grid-forming converter, UI, as represented in Fig. 1.

From (7), the active and reactive references of phase power flow at the PCC are set, respectively, to $P^*_{PCCm} = P_{UIm} = 11kW$ and $Q^*_{PCCm} = Q_{UIm} = 0$. The results of Fig. 9 show four intervals representing different events, while Table V reports the steady-state values of power corresponding these events. The power terms at PCC (*A*: apparent, *P*: active, *Q*: reactive, *N*: unbalance, *D*: distortion) are computed by means of the Conservative Power Theory (CPT) [36].

In interval #1, all DERs are disconnected, so the full MG load is supplied by the UI, which clearly characterizes asymmetric and distorted current waveforms, as quantified in Table V.

At time 0.55s (interval #2) the DERs are activated, and each inverter contributes phase-dependent with power (active and reactive) proportional to their capacity regardless of whether it is current-based or voltage-based controlled (see Table V). Still, the three-phase converter works balanced and provides power proportionally to the average between the necessity of the three phases. Thus, with DERs generating power, the UI reduces its active power feed-in, the reactive power circulation is reduced (Q_{PCC} is 0.51kVAR), as well as the current unbalance at the PCC (N_{PCC} reduction to 0.28kVA).

The interval #3, starting at time 0.65s, corresponds to set the active power of DER_6 connected to phases *ca* to zero ($P_{G6}^{max} = 0$). Which is equivalent to an APF operation. However, one can see that the unbalanced power remains small (N_{PCC}=0.38kVA). At 0.75s (interval #4), the DER_6 is completely turned-off and the UI instantaneously increases its current contribution in phase *c*. Nevertheless, the other DERs keep compensating the unbalanced power and, at steady-state, it is reached a low value of unbalanced power (N_{PCC}=0.24kVA) and reactive power (Q_{PCC}=0.86kVAr).

In addition, the system frequency remains constant and the voltage presents little variation while a proportional power sharing among the converters capability, within the same *m*-phase, is achieved (see Tables IV and V). For instance, at interval #4, the DERs connected at phases *ab* absorb 14 % of their maximum active power capacity, and DERs at phases *bc* inject 90 %. For reactive power, the inverters at phases *ab* contribute with 60 %, while the DERs at phases *bc* with 21 % of their corresponding maximum reactive power available.

In Fig. 10, the DERs active and reactive power all over the simulation are shown considering that the event #4 remains until 1.5 s. The power terms at the PCC are shown demonstrating that during the interval #4, the UI provides mainly active and distortion power (harmonics), and practically zero reactive and unbalanced power terms.

TABLE III
PARAMETERS OF THE THREE-PHASE FOUR-WIRE LOW-VOLTAGE MICROGRID

Line impedances		**Z[mΩ]**
From	**To**	
N_0	N_1	460+*j*1850
N_1, N_2, N_5, N_6	N_2, N_5, N_6, N_7	7.0+*j*9.7
N_2, N_3, N_7	N_3, N_4, N_8	48.3+*j*10.3
N_5, N_9	N_9, N_{12}	22.3+*j*11.4
N_9, N_{10}	N_{10}, N_{11}	20.3+*j*6.9
N_{12}	N_{13}	19.1+*j*9.8

TABLE IV
PARAMETERS OF THE DISTRIBUTED DERS

Parameters	**DER_j (N_3, N_4, N_6, N_8, N_{11}, N_{12})**
Power rating [kVA]	(5.0, 9.0, 18.0, 33.0, 16.0, 13.0)
Power capacity [kW]	(4.5, 8.0, 16.0, 22.5, 14.0, 11.0)
Max. power capacity [kW]	(4.5, 8.0, 16.0, 22.5, 14.0, 11.0)
Min. power capacity [kW]	-(4.5, 8.0, 16.0, 22.5, 14.0, 11.0)

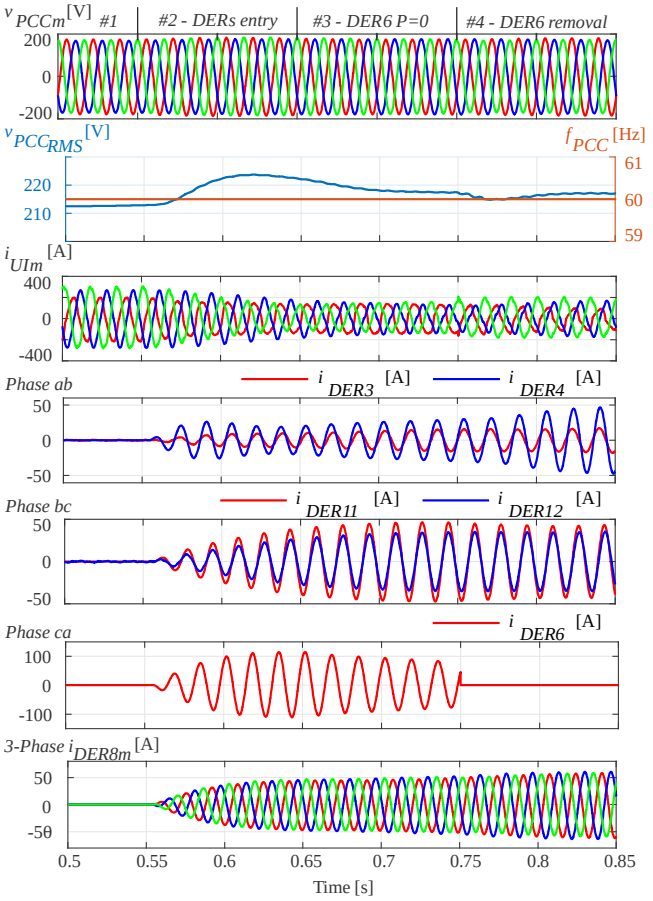

Fig. 9. Islanded microgrid operation with Power-Based Control under several sequential events.

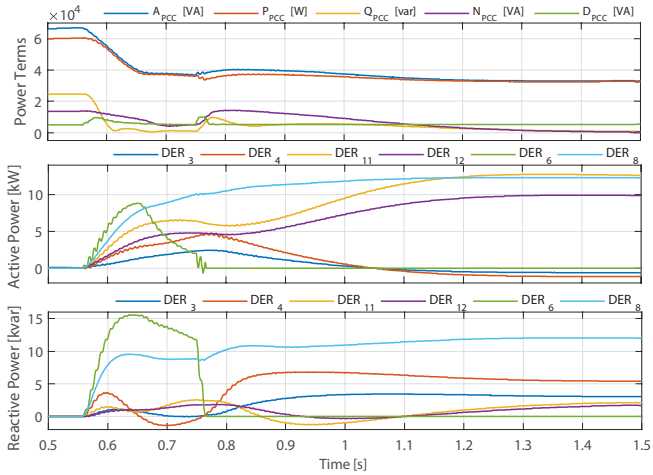

Fig. 10. Power terms at the PCC, DERs active and reactive power.

B. *Compliance with Steinmetz compensation*

Compliance with Steinmetz principle is herein discussed by simulations, being validated by experimental results in Section VI. Firstly, the circuit shown in Fig. 11 is simulated in PSIM software to compare the PBC strategy with the analytical equations described in Section IV. Note that DER_1 and DER_2 are, respectively, connected between phases *ab* and *bc*, and they have the same rated power of 6kVA. A balanced three-phase resistive load ($R_{3\Phi}$ = 146.1 Ω) is fed by a 220 V_{RMS} grid line voltage, and another resistive load ($R_{1\Phi}$ = 41.2 Ω) is connected between phases *ca* to emulate load unbalance. The grid line impedance (Z_{line}) is an inductance equal to 0.5 mH.

TABLE V
STEADY-STATE CPT'S POWER TERMS AT PCC AND DERS POWER MEASURES RELATED TO FIG. 9 AND FIG. 10

Parameters	(#1)	(#2)	(#3)	(#4)
A_{PCC} [kVA]	66.7	33.4	33.6	33.1
P_{PCC} [kW]	60.2	33.0	33.2	32.7
Q_{PCC} [kVAr]	24.6	0.51	0.51	**0.86**
N_{PCC} [kVA]	13.7	0.28	0.38	**0.24**
D_{PCC} [kVA]	5.1	5.1	5.1	5.3
DER_3 P[kW] ; Q[kVAr]	---	2.4; -0.5	2.9; 1.6	-0.6; 3.0
DER_4 P[kW] ; Q[kVAr]	---	4.3; -0.9	5.2; 2.9	-1.1; 5.4
DER_{11} P[kW] ; Q[kVAr]	---	5.1; 2.4	6.8; -0.4	12.6;2.2
DER_{12} P[kW] ; Q[kVAr]	---	4.0; 2.0	5.3; -0.2	9.9; 1.7
DER_6 P[kW] ; Q[kVAr]	---	7.3; 13	0 ; 12.3	---
DER_8 P[kW] ; Q[kVAr]	---	9.7; 8.9	12.3;8.8	12.3; 12

Regarding the implementation of the PBC method, the power reference signals are calculated by the MC (at the MG´s PCC), as well as by each DER´s controller, using voltages and currents measured as in Fig. 11, and transmitting the power terms through the communication link to the MC. However, for the equations of Section IV, also computed in the MC, the reference signals are calculated considering the estimated load power (4) and line-to-line voltages v_{ab} and v_{bc} as also indicated in Fig. 11. Yet, v_{ca} is obtained from the measurement of v_{ab} and v_{bc}, while the phase voltages are calculated using (10). Note that, since DERs are connected between phases *ab* and *bc*, only the terms P^*_{ab}, P^*_{bc}, Q^*_{ab} and Q^*_{bc} from $\underline{P}^*$ and $\underline{Q}^*$ are required to be calculated using (15) and (16.b).

In both simulated approaches, the DERs are not injecting any currents before t = 1.1s. After this instant, both DERs started performing unbalance and reactive power compensation until t = 1.4 s. Thereafter, DERs inject active power, while still performing compensation tasks. The following discussion is based on Figs. 12 and 13.

According to Steinmetz, in this circuit the currents become balanced if a capacitor and an inductor are placed between phases *ab* and *bc*, respectively. Nonetheless, by means of the PBC, the DERs connected in those phases may be actively coordinated to emulate such behaviors.

Considering the approach from Section IV, Table VI presents the power decomposition and power reference signals for this simulation. Since the supply voltages are symmetric, the balanced active power has the same value in the three phases. As the load is comprised only of resistive elements, $Q_{3\emptyset} = 0$, so the balanced components of the reactive power are also null. Therefore, the non-zero reactive power in the PCC phases correspond to the unbalanced reactive powers (i.e., $\underline{Q} = \underline{Q}^u$), and this may be explained by the circulation of currents with phase displacement in relation to phase voltages, which is caused by the resistor placed at phase *ca*.

According to Figs. 12 and 13, the current waveforms at the PCC have become almost balanced and in-phase with the supply voltages when 1.1 s < t < 1.4 s; and they are closer to zero when the DERs are injecting both active and reactive

TABLE VI
DECOMPOSITION OF ACTIVE AND REACTIVE POWER AND REFERENCE SIGNALS CALCULATED ACCORDING TO (14) AND (15.B)

DERs off	
$\underline{P}$	$[697.6 \quad 110.5 \quad 697.6]^T$ W
$\underline{P}^b$	$[501.9 \quad 501.9 \quad 501.9]^T$ W
$\underline{P}^u$	$[195.7 \quad -391.4 \quad 195.7]^T$ W
$P_{3\emptyset}$	1505.7 W
$\underline{Q} = \underline{Q}^u$	$[339.1 \quad 0 \quad -339.1]^t$ VAr
$Q_{3\emptyset}$	0.0
DERs operating as APFs	
$\underline{Q}^*$	$[678.1 \quad -678.1 \quad 0]^T$ var
Multifunctional operation of the DERs	
$\underline{P}^*$	$[501.9 \quad 501.9 \quad 0]^T$ W
$\underline{Q}^*$	$[678.1 \quad -678.1 \quad 0]^T$ var

power. Regarding the response time of the PBC operation, the power reference signals and injected powers reached steady-state after 6 cycles of fundamental frequency (60 Hz), which may be justified by the MC transmission rate of one cycle of 60 Hz and the iterative characteristic of the PBC algorithm. Moreover, note that the steady-state power components injected by each DER in each case are higher than the initial power reference signals, due to the closed-loop characteristic of the PBC: since that the remaining power components at PCC (either active or reactive) are summed up with the corresponding injected ones by each DER at every computation cycle, the reference signals would vary until the remaining powers at PCC are closer to zero.

On the other hand, the results presented for the application of the approach described in Section IV show effective compensation of unbalanced active and reactive power at PCC when 1.1 s < t < 1.4 s, which confirms that it is possible to compensate load unbalance of a purely resistive load using two converters. In fact, note that the power components injected by the DERs match the power reference signals after t = 1.1 s. However, since only two line-to-line DERs are available, it is not possible to provide total active power to the load. The remaining active power component at PCC, which should be addressed to a DER connected between phases *c* and *a*, is equal to 501.9 W. This value corresponds to the balanced active power component of one phase, and it is reflected in the three PCC phases in an unbalanced way, which can be observed in the PCC currents after t = 1.4 s in Figs. 14 and 15.

VI. EXPERIMENTAL RESULTS

The experimental results validate the current unbalance compensation devised by single-phase DERs, certify the mathematical analysis described in Section IV, and assesses the PBC operation according to the Steinmetz approach [26], [37] as discussed in Section V-B. Aiming such goal, an experimental setup shown in Fig. 16(a) is assembled comprising two single-phase 6 kVA DERs with *L*-filters, being coupled to different phases of a three-phase three-wire LV network as in Fig. 11, and responding to commands to share active, reactive and unbalanced power terms as described in Section III. Table VII

TABLE VII
DER AND GRID PARAMETERS FOR THE EXPERIMENTAL RESULTS

Feature	Specification
Grid nominal voltage (line-line)	220 V_{RMS} @ 60Hz
Grid line impedance (Z_{line})	0.5 mH
DC Link voltage of DERs (V_{DC1}=V_{DC2})	400 V
L filters of DERs (L_{g1}=L_{g2})	1.0 mH
Switching (f_{sw}) and sampling (f_s) frequencies	12 kHz
Current sensor gain (K_i)	1/25
PRes proportional (K_{Pi}) and integral (K_{Ih}) gains	1.0 and 430

shows the system parameters.

Following the circuit presented in Fig. 11, the mains is devised by a *Regatron* four-quadrant grid simulator, and line impedances (Z_{line}) are placed between the mains and the PCC to emulate a network with high X/R ratio, representing a realistic scenario comprising likely voltage deviations over line inductances. As aforementioned, PCC phase voltages ought to be measured with reference to a virtual point, or they could be attained from line-to-line measurements. Herein, the latter is chosen, requiring phase voltages to be calculated from line voltages as given in (10).

The DC links of DERs are supplied by programmable DC sources. Current and voltage measurements are attained by *LEM* sensors. The PBC algorithm and proportional-resonant (PRes) current controllers, designed for each DER as in [38], are implemented within a TMS320F28335 floating-point digital signal processor (DSP). *DPO3014* and *MSO2014 Tektronix* oscilloscopes are used to acquire the experimental results. One cycle of the 60 Hz fundamental grid voltage (i.e., 16.67 ms) is chosen for the periodic communication between the MC and DERs. It is highlighted that only one DSP is used for the experiments, with the implemented coding logic summarily presented in Fig. 16(b); consequently, transmission delays and data packet loss are neglected.

The compliance with Steinmetz's principle is shown by two case studies: on the first, DERs only perform compensation; and on the second, they additionally share active power. Initially, Fig. 17(a) shows the practical result of the circuit described in Figs. 11 and 16(a), demonstrating the line voltage v_{ab} and PCC currents, with DERs disabled. It is clearly seen the unbalanced power flow through the PCC, with three-phase apparent and active power respectively equal to 1.92 kVA and 1.51 kW, computed as in [36]. The maximum difference of apparent power between any two phases (ΔA_{max}) is approximately 619 VA. Yet, by means of Fig. 17(a) and Fig. 18, it is noticeable that the magnitudes of the PCC currents are initially unbalanced, presenting absolute phase deviation of 28.17° and 24.3°, for phases *a* and *c*, in relation to the expected 0° and 120° referred to V_a^*. Total harmonic distortion of PCC currents (THDi) is 1.60 %, 1.92%, and 1.73 %, respectively for phases *a*, *b* and *c*.

The first case study, Figs. 17(b) to 17(f) present the results of this operation considering transient and steady-state conditions, demonstrating that two distributed single-phase DERs can share active/reactive power and compensate unbalanced current terms. For this case, DERs start with null reference, injecting

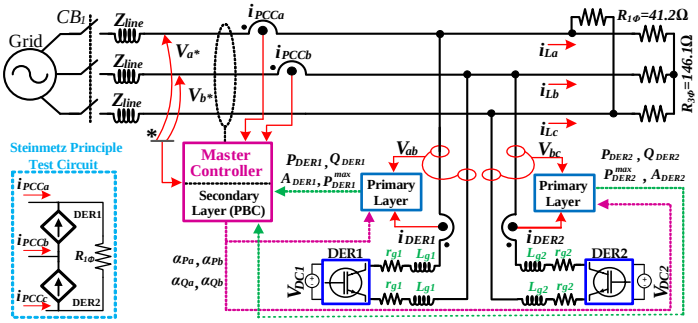

Fig. 11. Circuit adopted for simulations of compliance with Steinmetz principle.

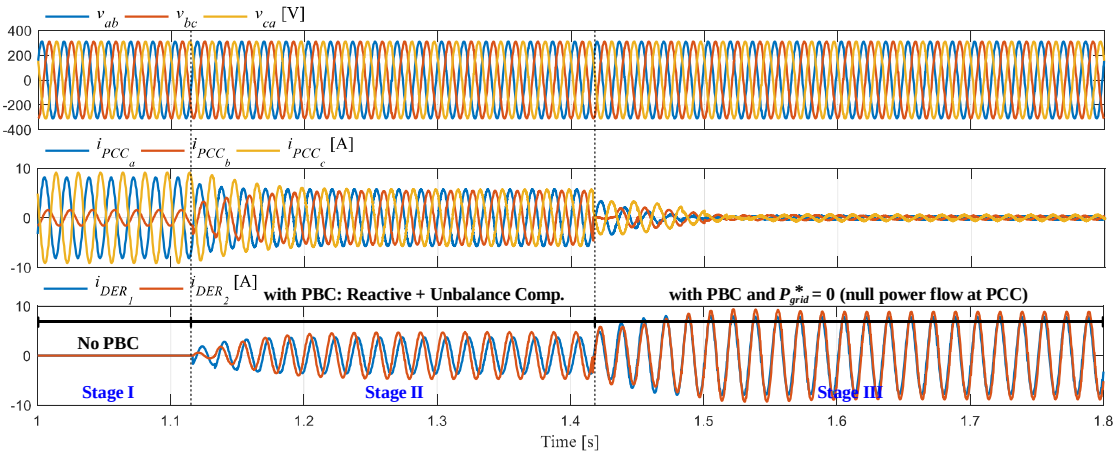

Fig. 12. Line-to-line voltages and currents at PCC, and DER currents according to the PBC applied to the test circuit for compliance with the Steinmetz approach.

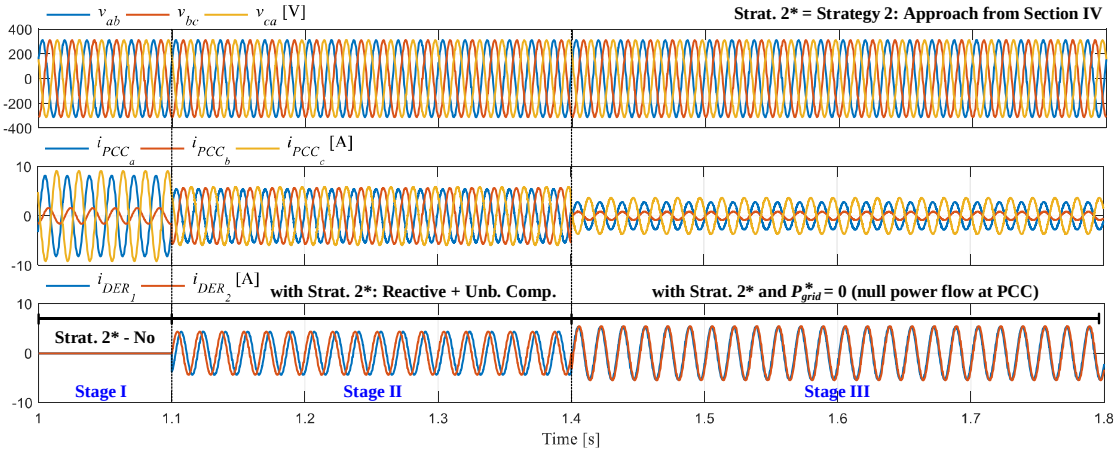

Fig. 14. Line-to-line voltages and phase currents at PCC, and DER currents according to the calculated using (15) and (16.b).

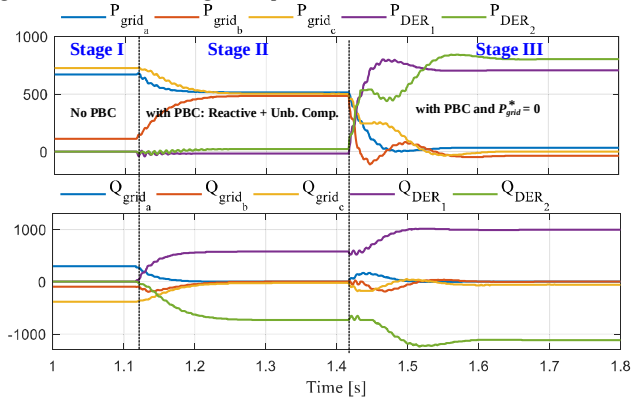

Fig. 13. PCC and DER active and reactive power according to the PBC applied to the test circuit for compliance with the Steinmetz approach.

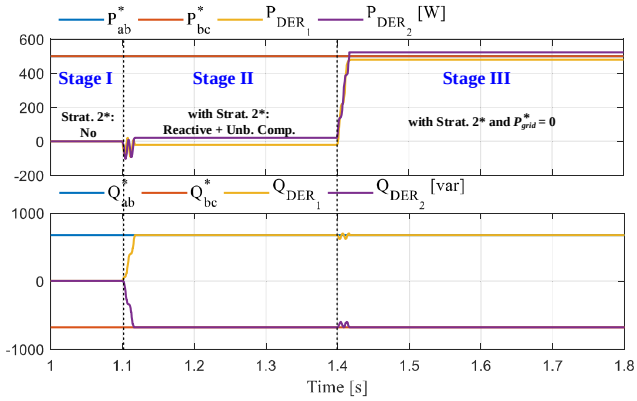

Fig. 15. Power reference signals calculated using (15) and (16.b) and injected power by each DER for compliance with the Steinmetz approach.

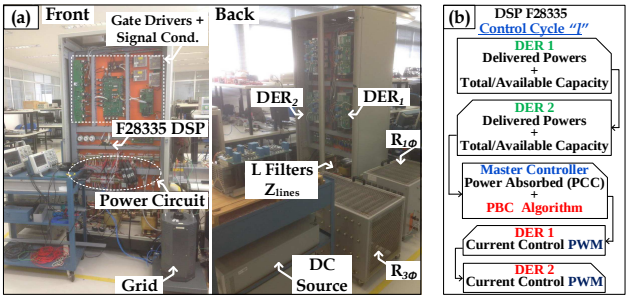

Fig. 16. (a) Experimental setup assembled for validation results; and (b) summary of the coding sequence devised in F28335 DSP.

currents with neglected fundamental amplitude. Thus, when the PBC is achieved, they start to share reactive and unbalance power terms, and the PCC and DERs currents smoothly change (see Figs. 17(b) to 17(d)) to steady-state (see Figs. 17(e) and 17(f)) without impairing in neither overvoltage nor overcurrent. As aforementioned, the PBC steers DER_1 to emulate an inductor, whereas DER_2 is driven as a capacitor, likewise expected by the Steinmetz principle.

As depicted in Fig. 18, the apparent power drawn at each phase is now less uneven among themselves, alike the magnitudes of the PCC currents. Also, comparing to the previous currents drawn by the loads, it results in lower phase deviation of PCC currents in relation to phase voltages, presenting reduction of 7.83° and 31.8° respectively for phases *a* and *c*. Additionally, ΔA_{max} is 107 VA, which shows a reduction of approximately 5.8 times in comparison to the initial case, also indicating the power balance among phases. Although the resulting currents circulating at the PCC show THDi of 8.6 %, 13.2 % and 7.1 %, such distortions are mainly consequence of some harmonic content on DERs currents caused by the improper filtering of the iron-core *L* inductors used, and due to low signal-to-noise ratio on signal conditioning. Finally, it is summarized that under such case study, the PBC drives the DERs as distributed APFs, compensating non-active power. Hence, with significant compensation of non-active power terms, it can be inferred that mostly active power is flowing through the PCC.

Another scenario (i.e., case study 2) is presented with the same DERs operating as multifunctional inverters, complementarily providing active power injection along with the ancillary reactive and unbalanced power sharing. For this experiment, the PBC processes the total amount of active and reactive power flowing through the phases and computes the amount of energy that should be injected by the two DERs to attain zero power flow at the PCC. Similarly to the previous case, the transient of this operation is depicted in Figs. 17(g) to 17(i), with steady-state shown in Figs. 17(j) and 17(k), considering DERs with null initial current control references. Upon the initialization of the PBC algorithm to share active and non-active power terms, PCC currents start to decrease up to a steady-state condition (see Figs. 17(g), 17(h) and 17(j)) with amplitudes much lower than the initial stage, presenting as remaining apparent power of 116, 136, 78 VA respectively for phases *a*, *b* and *c* as seen in Fig. 18. The maximum variation of apparent power between phases is ΔA_{max} = 58 VA, being approximately 10 times lower than on the initial unbalanced condition. Note that, for both experimental scenarios, the system presented similar frequency response (i.e., 6 to 7 fundamental cycles to reach steady-state) and the PBC is able to share the active and reactive power demanded by loads, allowing also compliance with the Steinmetz principle by steering two arbitrarily connected single-phase DERs to mitigate current unbalance.

VII. Conclusions

This paper contributes with a coordinated strategy accommodating three-phase and single-phase DERs coexisting in a low-voltage microgrid. Such three-phase DERs operate in balanced mode, contributing to the MG's active and reactive power demand, avoiding re-sizing their DC capacitors. Single-phase DERs contribute to active feed-in, plus reactive and unbalance compensation (negative-sequence), without impairing voltage quality. Thus, in a three-phase three-wire network, using only two single-phase distributed inverters it is possible to support balanced power flow at the MG's PCC.

Despite of its possible drawbacks, given by its communication dependence and relatively higher costs, centralized master/slave architectures provide more precise controllability, not imposing voltage/frequency deviations, and eliminating the use of additional compensating devices. For instance, the proposed PBC avoids overcurrent stresses and allow power constraints to be dealt locally, easily complying with grid codes and converter limitations.

Simulation results show the efficient and stable operation under several typical conditions, such as: islanded and grid-connected modes, and power and local variation. The experimental results validate the control strategy and its compliance with Steinmetz Theorem.

References

[1] D. I. Brandao, T. Caldognetto, F. P. Marafão, M. G. Simões, J. A. Pomilio, and P. Tenti, "Centralized Control of Distributed Single-Phase Inverters Arbitrarily Connected to Three-Phase Four-Wire Microgrids," *IEEE Trans. Smart Grid*, vol. 8, no. 1, pp. 437–446, 2017.

[2] R. Tonkoski, D. Turcotte, and T. H. M. EL-Fouly, "Impact of high PV penetration on voltage profiles in residential neighborhoods," *IEEE Trans. on Sustain. Energy*, vol. 3, no. 3, pp. 518–527, July 2012.

[3] J. Rocabert, A. Luna, F. Blaabjerg, and P. Rodriguez, "Control of power converters in AC microgrids," *IEEE Trans. Power Electron*., vol. 27, no. 11, pp. 4734–4749, Nov. 2012.

[4] J. P. Bonaldo, H. K. M. Paredes, and J. A. Pomilio, "Control of single-phase power converters connected to low-voltage distorted power systems with variable compensation objectives," *IEEE Trans. Power Electron*., vol. 31, no. 3, pp. 2039–2052, 2016.

[5] Z. Zeng, X. Li, and W. Shao, "Multi-functional grid-connected inverter: upgrading distributed generator with ancillary services," *IET Renew. Power Gener*., vol. 12, no. 7, pp. 797–805, 2018.

[6] W. Choi, W. Lee, D. Han, and B. Sarlioglu, "New Configuration of Multifunctional Grid-Connected Inverter to Improve Both Current-Based and Voltage-Based Power Quality," *IEEE Trans. Ind. Appl*., vol. 54, no. 6, pp. 637 6382, 2018.

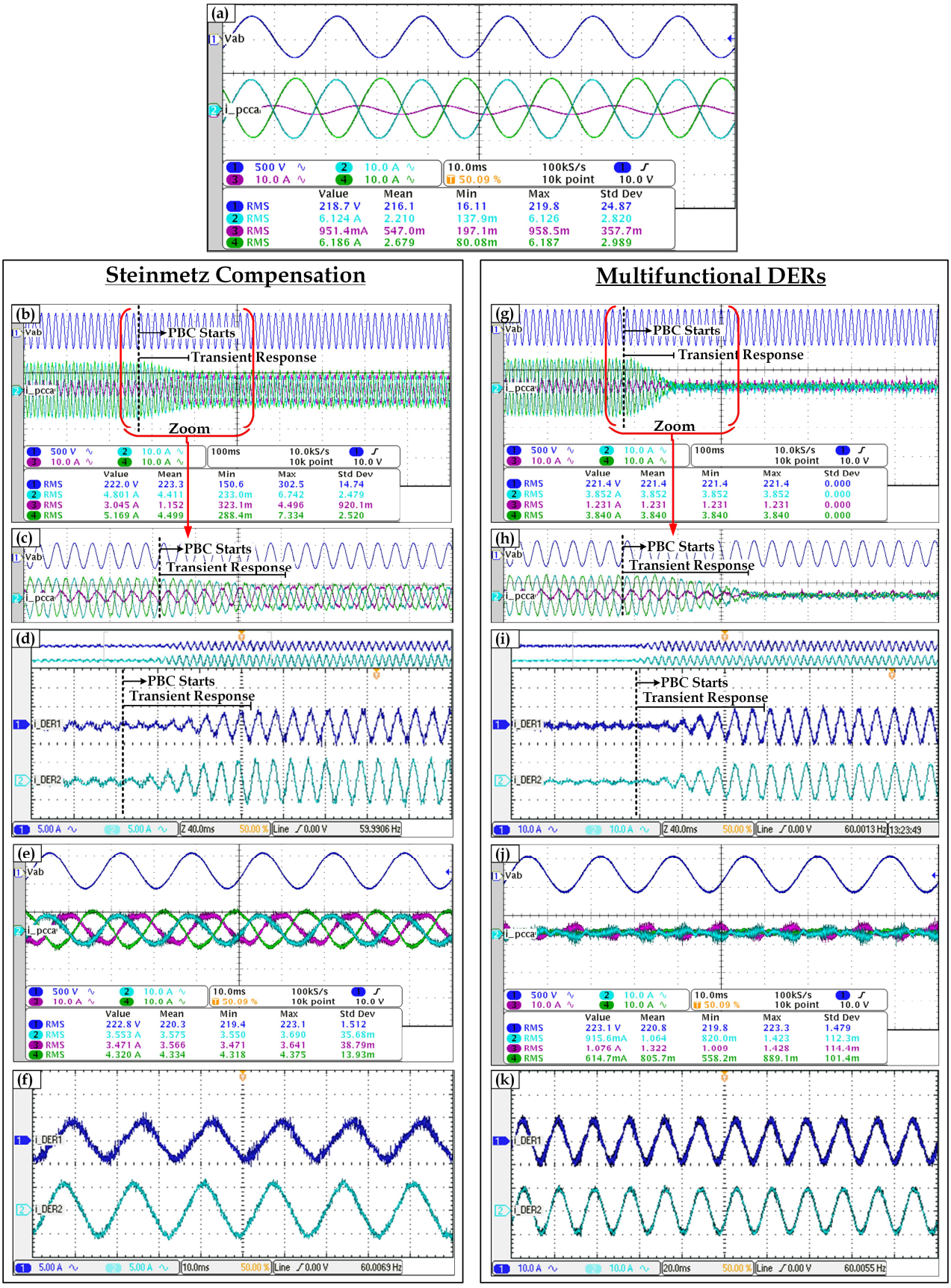

Fig. 17. Experimental results of DER and PCC quantities: (a) PCC line-to-line voltage and currents considering DERs disabled; (b) to (f) transient and steady-state results for the Steinmetz compensation; (g) to (k) transient and steady-state results for DERs driven as multifunctional inverters by the PBC algorithm.

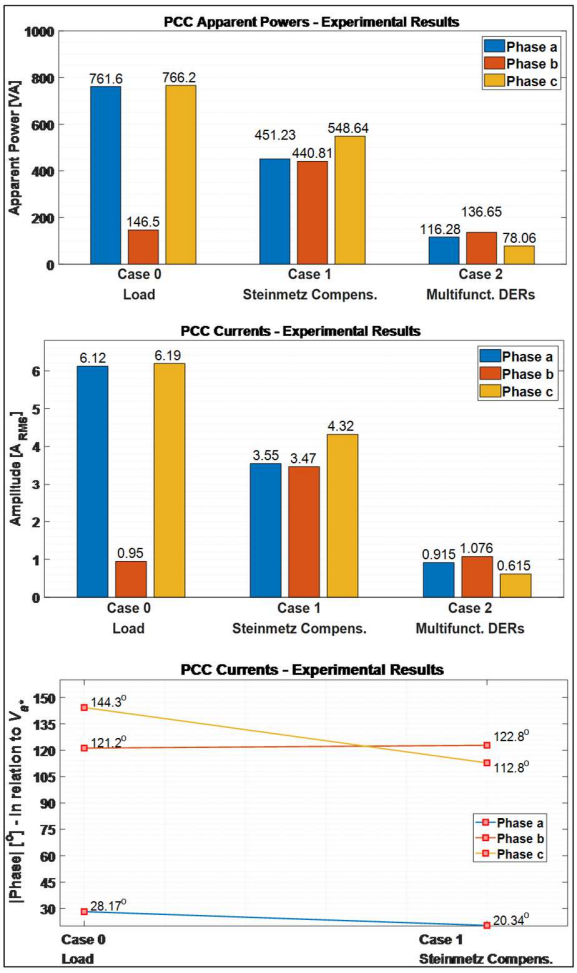

Fig. 18. Apparent power per-phase, current magnitudes and phase deviation of currents at the PCC for the experimental results.

[7] Z. Ali, N. Christofides, L. Hadjidemetriou, and E. Kyriakides, "Diversifying the Role of Distributed Generation Grid Side Converters for Improving the Power Quality of Distribution Networks using Advanced Control Techniques," *IEEE Trans. Ind. Appl.*, vol. 55, no. 4, pp. 4110–4123, 2019

[8] Z. Ali, N. Christofides, L. Hadjidemetriou, and E. Kyriakides, "Multi-functional distributed generation control scheme for improving the grid power quality," *IET Power Electron*., vol. 12, no. 1, pp. 30–43, 2018.

[9] Institute of Electrical and Electronics Engineers, IEEE Standard 1547 for Interconnection and Interoperability of Distributed Energy Resources with Associated Electric Power Systems Interfaces. 2018.

[10] C. Ahumada, R. Cárdenas, D. Sáez and J. M. Guerrero, "Secondary Control Strategies for Frequency Restoration in Islanded Microgrids With Consideration of Communication Delays," *IEEE Transactions on Smart Grid*, vol. 7, no. 3, pp. 1430-1441, 2016.

[11] Q. Sun, J. Zhou, J. M. Guerrero, and H. Zhang, "Hybrid Three-Phase / Single-Phase Microgrid," *IEEE Trans. Power Electron*., vol. 30, no. 10, pp. 5964–5977, 2015.

[12] Y. A.-R. I. Mohamed and E. F. El-Saadany, "Adaptive decentralized droop controller to preserve power sharing stability of paralleled inverters in distributed generation microgrids," *IEEE Trans. Power Electron*. vol. 23, no. 6, pp. 2806–2816, Nov. 2008.

[13] W. Yao, M. Chen, J. M. Guerrero, and Z.-M. Qian, "Design and analysis of the droop control method for parallel inverters considering the impact of the complex impedance on the power sharing," *IEEE Trans. Ind. Electron*., vol. 58, no. 2, pp. 576–588, Feb. 2011.

[14] M. Ashabani, Y. A. R. I. Mohamed, M. Mirsalim, and M. Aghashabani, "Multivariable Droop Control of Synchronous Current Converters in Weak Grids/Microgrids with Decoupled dq-Axes Currents," *IEEE Trans. Smart Grid*, vol. 6, no. 4, pp. 1610–1620, 2015.

[15] C. Blanco, D. Reigosa, J. C. Vasquez, J. M. Guerrero, and F. Briz, "Virtual admittance loop for voltage harmonic compensation in microgrids," *IEEE Trans. Ind. Appl.*, vol. 52, no. 4, pp. 3348–3356, Jul./Aug. 2016.

[16] M. Zeraati, M. E. H. Golshan, and J. M. Guerrero, "Voltage Quality Improvement in Low Voltage Distribution Networks Using Reactive Power Capability of Single-Phase PV Inverters," *IEEE Trans. Smart Grid*, vol. PP, no. c, p. 1, 2018.

[17] A. Ranjbaran and M. Ebadian, "A power sharing scheme for voltage unbalance and harmonics compensation in an islanded microgrid," *Electr. Power Syst. Res*., vol. 155, pp. 153–163, 2018.

[18] T. Caldognetto, S. Buso, P. Tenti and D. Brandao, "Power-based control of low-voltage microgrids," *IEEE Journal of Emerging and Selected Topics in Power Electronics*, vol. 3, no. 4, pp. 1056-1066 , Oct. 2015.

[19] D. I. Brandao, L. S. de Araújo, T. Caldognetto, and J. A. Pomilio, "Coordinated control of three- and single-phase inverters coexisting in low-voltage microgrids," *Appl. Energy*, vol. 228, no. March, pp. 2050–2060, 2018.

[20] S. Y. M. Mousavi et al, "Autonomous Control of Current and Voltage Controlled DG Interface Inverters for Reactive Power Sharing and Harmonics Compensation in Islanded Microgrids," *IEEE Trans. Power Electron*., vol. 33, no. 11, pp. 9375-9386, 2018.

[21] M. Savaghebi, A. Jalilian, J. C. Vasquez, and J. M. Guerrero, "Autonomous voltage unbalance compensation in an islanded droop-controlled microgrid," *IEEE Trans. Ind. Electron*., vol. 60, no. 4, pp. 1390–1402, 2013.

[22] P. T. Cheng, C. A. Chen, T. L. Lee, and S. Y. Kuo, "A cooperative imbalance compensation method for distributed-generation interface converters," *IEEE Trans. Ind. Appl.*, vol. 45, no. 2, pp. 805–815, 2009.

[23] M. Savaghebi, A. Jalilian, J. C. Vasquez, and J. M. Guerrero, "Secondary control scheme for voltage unbalance compensation in an Islanded droop-controlled microgrid," *IEEE Trans. Smart Grid*, vol. 3, no. 2, pp. 797–807, 2012.

[24] M. Savaghebi, A. Jalilian, J. C. Vasquez, and J. M. Guerrero, "Secondary control for voltage quality enhancement in microgrids," *IEEE Trans. Smart Grid*, vol. 3, no. 4, pp. 1893–1902, 2012.

[25] S. Y. Mousazade Mousavi, A. Jalilian, M. Savaghebi, and J. M. Guerrero, "Coordinated control of multifunctional inverters for voltage support and harmonic compensation in a grid-connected microgrid," *Electr. Power Syst. Res*., vol. 155, pp. 254–264, 2018.

[26] L. Gyugyi, R. A. Otto, and T. H. Putman, "Principles and Applications of Static, Thyristor-Controlled Shunt Compensators," *IEEE Trans. Power Appar. Syst*., vol. 75, no. 5, 1978.

[27] Worldstandards (2019, April). Three-phase electric power: industrial application only. Available in: https://www.worldstandards.eu/three-phase-electric-power/.

[28] L. Henry, "Design and implementation of off-grid systems," in Off-Grid Electrical Systems in Developing Countries, 1st ed.: Springer International Publishing, 2018, ch 12, pp. XXIII, 481.

[29] P. Tenti, T. Caldognetto, S. Buso, and D. I. Brandão, "Control Of Utility Interfaces In Low-voltage Microgrids," *Brazilian Power Electron. Journal*., vol. 20, no. 4, pp. 373–382, 2015.

[30] Solar Inverters Product Catalogue. Available in: http://pdf.archiexpo.com/pdf/delta-energy-systems/solar-inverters-product-catalogue/88145-251418.html.

[31] Y. Mohamed and A. A. Radwan, "Hierarchical control system for robust microgrid operation and seamless mode transfer in active distribution systems," *IEEE Trans. Smart Grid*, vol. 2, no. 2, pp. 352–362, 2011.

[32] T. O. Kowalska, F. Blaabjerg, J. Rodríguez, Advanced and Intelligent Control in Power Electronics and Drives, Springer Inter. Publish., 2014.

[33] American National Standards Institute, "ANSI C84.1-American National Standard for Electric Power Systems and Equipment—Voltage Ratings (60 Hz)," Oct. 2016.

[34] A. Angioni, A. Sadu, F. Ponci, A. Monti, D. Patel, F. Williams, D. della Giustina and A. Dedè, "Coordinated Voltage Control in Distribution Grids with LTE Based Communication Infrastructure," in Proc. IEEE Int. Conf. Environ. Elec. Eng., Rome, Italy, 2015, pp. 2090-2095.

[35] K. Ogata, Discrete-time Control Systems, 2nd ed., Prentice-Haal, NJ, 1994.

[36] P. Tenti, H. M. Paredes, and P. Mattavelli, "Conservative power theory, a framework to approach control and accountability issues in smart microgrids,"*IEEE Trans. Power Electron*.,vol.26,no.3,pp.664–673, 2011.

[37] Li. Monjo, L. Sainz, S. Riera and J. Bergas, "Theoretical Study of the Steinmetz Circuit Design," *Electric Power Components and Systems*, vol. 41, no 3, pp. 304-323, Jan. 2013.

[38] S. Buso and P. Mattavelli, "Digital Control in Power Electronics," 2nd Ed., Morgan & Claypool, 2015.

Danilo I. Brandao (S'14-M'16) received the Dr. degree in Electrical Engineering from University of Campinas, Brazil, in 2015. He was a visiting scholar at Colorado School of Mines, USA, in 2009 and in 2013, and at University of Padova, Italy, in 2014, and a guest professor at Norwegian University of Science and Technology, Norway, in 2018. He is currently assistant professor at Federal University of Minas Gerais with the Graduate Program in Electrical Engineering. His main research interests are control of grid-tied converters and microgrids. Mr. Brandao is a member of SOBRAEP and IEEE.

Lucas S. Araujo (S'19) is a PhD Student in Electrical Engineering at Federal University of Minas Gerais (UFMG), with Master's degree in Electrical Engineering at University of Campinas (2017), and bachelor degree in Electrical Engineering at the Federal University of Uberlandia (2013). Industry experience as a Project Engineer. His areas of interest are: power electronics, renewable energy, distributed generation, smart and microgrids, energy storage systems and electric vehicles.

Augusto M. S. Alonso (S'16) received the M.S. degree in Electrical Engineering from the São Paulo State University (UNESP), Brazil, in 2018. Currently, he is working toward a double Ph.D. degree at UNESP and at the Norwegian University of Science and Technology (NTNU), Norway. He was a visiting scholar at the University of New Mexico, USA, during 2012-2013. His main interests are coordinated control of grid-tied converters, hierarchical microgrid control, and power quality, and energy policies.

Geovane L. dos Reis (S'16) received the B.S. degree in electrical engineering from the Federal University of Itajubá (UNIFEI), Campus Itabira, Brazil, in 2014 and the M.S. degrees in electrical engineering from the Federal University of Minas Gerais (UFMG), where he is currently working toward the Ph.D. degree. Currently he is an Assistant Professor at the Federal University of Itajubá (UNIFEI), Campus Itabira. His main research interests include power electronic applications in renewable energy, coordinated control of grid-tied converters, hierarchical microgrid control and power quality.

Eduardo V. Liberado (S'08-M'19) received the Dr. degree in Electrical Engineering from University of Campinas, Brazil, in 2017. He was a visiting scholar at University of Padova, Italy, in 2013. He is currently an Assistant Professor at São Paulo State University, Campus of Rosana, with the Bioenergy and Sustainable Energies research group (Biojoule). His current research interests include application of power conditioning systems in smart grids under non-sinusoidal and unbalanced conditions; and numerical simulation of renewable energy sources.

Fernando P. Marafão (S'95–M'05) received the B.S. degree in electrical engineering from UNESP, Brazil, in 1998, and the M.Sc. and Ph.D. degrees from UNICAMP, Brazil, in 2000 and 2004, respectively. In 2002, he joined the Power Electronics Group, University of Padova, Italy, as a visiting student. In 2013, he joined the Colorado School of Mines, USA, as a Visiting Scholar on Autonomous and Intelligent Distributed Energy Systems. Since 2005, he has been with UNESP, as an Associate Professor with the Group of Automation and Integrating Systems. His current research interests include smart grid technologies, renewable energies, energy management and power theories. He is a member of SOBRAEP, SBA and IEEE.